Numerical Calculation of Unsteady Transonic Potential Flow over Three-Dimensional Wings with Oscillating Control Surfaces

Koji Isogai*
National Aerospace Laboratory, Tokyo, Japan
and
Kohei Suetsugu†
FACOM-HITAC Inc., Tokyo, Japan

Numerical calculations of the unsteady transonic potential flow over three-dimensional wings with oscillating control surfaces are performed. For this purpose, a new grid system, which is appropriate for solving the control surface problems, is introduced into the computer code USTF3, which solves the unsteady three-dimensional full potential equation by a two-step semi-implicit time-marching technique. To validate the code, the unsteady pressure distributions on the NLR swept tapered wing with an inboard control surface and on the RAE swept tapered wing with a part-span control surface are calculated and compared with those of existing theories and experimental data. The qualitative behaviors of the unsteady pressure distributions due to the control surface oscillation are well predicted by the present method, but some quantitative discrepancies due to the viscous effects in the experiment are observed for supercritical Mach numbers.

Nomenclature

AR = aspect ratio
b = local semichord
b_0 = root semichord
C_0 = root chord
$\bar{C}$ = mean aerodynamic chord
C_p = pressure coefficient, $(p-p_\infty)/(1/2\rho_\infty Q_\infty)$
ΔC_p = pressure loading coefficient $(C_p^L - C_p^U)$
$C_{p,\theta}$ = first harmonic component (in complex form) of local pressure coefficient per unit θ $(C_{p,\theta} = C'_{p,\theta} + iC''_{p,\theta})$
$\Delta C_{p,\theta}$ = first harmonic component (in complex form) of local pressure loading coefficient per unit θ $(\Delta C_{p,\theta} = \Delta C'_{p,\theta} + i\Delta C''_{p,\theta})$
$f\langle x,z,t\rangle$ = y coordinate of instantaneous position of wing surface
k = reduced frequency based on root semichord $(k = b_0\omega/Q_\infty)$
M_∞ = freestream Mach number
p = pressure
q = dimensionless total velocity
Q = total velocity
R_{C_0} = Reynolds number based on root chord
s = dimensionless semispan
T = time
t = dimensionless time, $t = (Q_\infty/b_0)T$
U,V,W = dimensionless local velocity components in x, y, and z directions, respectively
x,y,z = dimensionless Cartesian coordinates in physical space
α = angle of attack
θ = amplitude of control surface oscillation
λ = taper ratio
Λ = sweep angle
ξ,η,ζ = dimensionless Cartesian coordinates in computational space
ρ = flow density
ϕ = dimensionless perturbation velocity potential
ω = circular frequency
$|\ |$ = absolute value

Subscripts

i,j,k = mesh point indices in ξ, η, and ζ directions, respectively
U,L = upper and lower surface of wing
∞ = freestream condition

Superscripts

n = time level index
U,L = upper and lower surface of wing

Introduction

THEORETICAL prediction of the unsteady aerodynamic forces on a three-dimensional (3D) wing with an oscillating control surface is of great importance, not only for its application to flutter analyses, but also for the design and evaluation of active control systems (such as active flutter suppression and gust load alleviation systems). Although several lifting surface theories[1-4] for predicting the unsteady subsonic aerodynamic forces due to a control surface oscillation have been presented, no reliable calculation method applicable to the transonic regime has yet been established.

Recently, however, several numerical methods[5-11] for predicting unsteady transonic aerodynamic forces on an oscillating 3D wing have been proposed. It is clear that these methods (or computer codes) can easily be extended to handle the oscillating control surface by introducing the appropriate grid systems.

In the present report, the computer code USTF3 developed by the present authors,[10,12] which solves the unsteady 3D full potential equation in quasilinear form by a two-step semi-implicit time-marching technique, has been extended to include the capability of calculating the unsteady transonic aerodynamic forces due to control surface oscillation.

Numerical Method

In this section, the outline of the basic equations and the finite difference scheme employed in USTF3 is given briefly. (Further details can be seen in Ref. 10.)

Received Jan. 18, 1983; revision received June 2, 1983.

*Head, Aeroelasticity Section. Member AIAA.
†System Engineer.

Basic Equations

The 3D unsteady full potential equation in quasilinear form can be written in Cartesian coordinates as

$$(a^2-U^2)\phi_{xx}+(a^2-V^2)\phi_{yy}+(a^2-W^2)\phi_{zz}-2UV\phi_{xy}$$
$$-2VW\phi_{yz}-2WU\phi_{xz}-2U\phi_{xt}-2V\phi_{yt}-2W\phi_{zt}-\phi_{tt}=0 \quad (1)$$

where the perturbation velocity potential ϕ can be related with the local velocity components U, V, and W in x, y, and z directions as

$$U=\phi_x+\cos\alpha, \qquad V=\phi_y+\sin\alpha, \qquad W=\phi_z \quad (2)$$

respectively, and where α is the mean angle of attack of the wing.

The local velocity of sound a in Eq. (1) can be given by

$$a^2=1/M_\infty^2-(\gamma-1)/2(2\phi_t+q^2-1) \quad (3)$$

where q is the total velocity. The pressure coefficient C_p can be calculated by using the following relation:

$$C_p=2\{[1+(\gamma-1)/2M_\infty^2(1-2\phi_t-q^2)]^{\gamma/(\gamma-1)}-1\}/(\gamma M_\infty^2) \quad (4)$$

In Eqs. (1-4), all of the physical quantities are nondimensionalized by the root semichord and a freestream total velocity Q_∞.

Let the wing be located near the $y=0$ plane and be oscillating normal to the x-z plane (see Fig. 1). Then, the flow tangency condition can be written as

$$V=f_t+Uf_x+Wf_z \quad (5)$$

where $f\langle x,z,t\rangle$ is the y coordinate of the instantaneous position of the wing surface. When we assume the amplitude of the wing oscillation is small, Eq. (5) can be satisfied at the time mean contour of the wing surface instead of at the exact location of the wing surface.

In order to simplify the treatment of the Kutta and wake boundary conditions, the wake is assumed to be located on the $y=0$ plane behind the trailing edge of the wing. With this assumption and the conditions of zero pressure difference at the trailing edge and across the wake, the following simplified form of the Kutta and wake boundary conditions can be derived by using Eq. (4) and retaining only the first-order terms:

$$\Delta\phi_t+\Delta\phi_x=0 \text{ on } y=0, \qquad x\geq x_t\langle z\rangle, \qquad |z|\leq s \quad (6)$$

where $\Delta\phi$ is the difference of the potential across the wake.

At the far field, the undisturbed flow conditions are imposed throughout the steady and unsteady calculations. At $z=0$ plane, the following symmetry condition is imposed:

$$W=0 \text{ on } z=0 \quad (7)$$

Grid System

The grid system employed in the present control surface calculations is a modification of that used in Ref. 10 and is shown schematically in Fig. 1. It is a stretched Cartesian grid system in the x-y plane and a stretched sheared grid system in the x-z plane. As shown in Fig. 1, x_H defines the percent semichord location of the hinge line in the streamwise direction, and z'_{H1} and z'_{H2} define the percent semispan locations of the control surface. In the figure, s is the semispan and $x_t\langle z\rangle$ and $x_t\langle z\rangle$ are the x coordinates of the leading and trailing edges and their smooth extensions of the far-field boundary in the z direction, respectively.

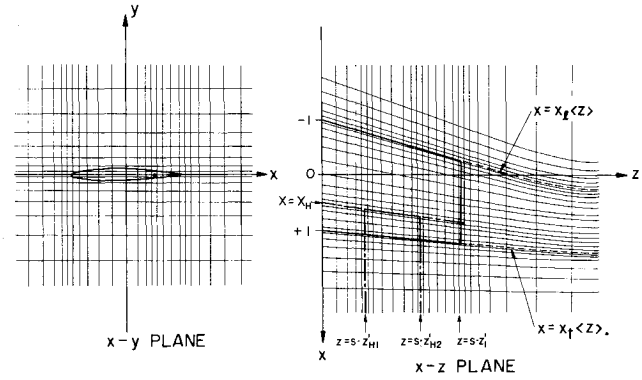

Fig. 1 Grid system in physical space (schematic).

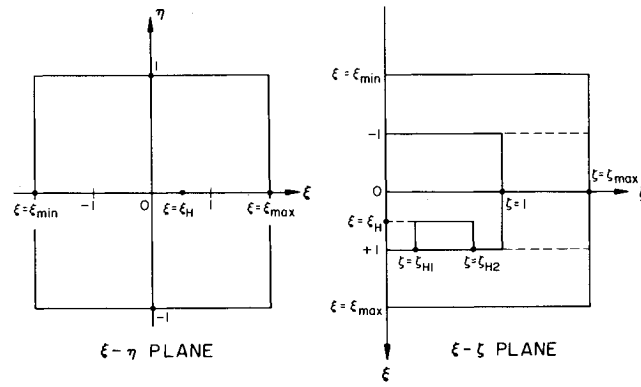

Fig. 2 Computational space.

An important point, which must be taken into account in generating a grid system for a control surface problem, is to locate the hinge line and the side edges of the control surface at about the midpoints of the adjacent grid lines, respectively, as shown in Fig. 1. In our previous experience in calculating the unsteady aerodynamic forces on a 2D airfoil with an oscillating control surface,[13] erroneous unsteady pressure distributions were obtained if the hinge line was not located approximately at the midpoint of the adjacent grid points. Keeping this fact in mind, we introduce the simple algebraic transformation functions to generate the grid system shown in Fig. 1, which transform the physical domain in x-y-z space into a computational domain in ξ-η-ζ space as shown in Fig. 2. The detailed form of the transformation functions are given in Ref. 14. These transformation functions are constructed so that the hinge line and the side edges of the control surface are located at the midpoints of the adjacent grid lines and so that the specified number of grid points can be distributed on the control surface.

Once the transformation functions are determined, the derivatives in the physical x-y-z space can be transformed into those of ξ-η-ζ space by the following relations:

$$\begin{bmatrix}\partial/\partial x\\ \partial/\partial y\\ \partial/\partial z\end{bmatrix}=\begin{bmatrix}f & 0 & 0\\ 0 & g & 0\\ h_1 & 0 & h_3\end{bmatrix}\begin{bmatrix}\partial/\partial\xi\\ \partial/\partial\eta\\ \partial/\partial\zeta\end{bmatrix} \quad (8)$$

where f, g, h_1, and h_3 are defined by

$$f=1/x_\xi, \quad g=1/y_\eta, \quad h_1=-x_\zeta/(x_\xi z_\zeta), \quad h_3=1/z_\zeta \quad (9)$$

Using these transformations [Eqs. (8)], the velocities and the derivatives of the perturbation velocity potential in the physical space can easily be expressed in terms of ξ, η, and ζ.

Finite Difference Scheme

The finite difference scheme employed in the present method is a two-step semi-implicit time-marching technique similar to that used in Ref. 15 for solving the two-dimensional unsteady transonic small-perturbation equation.

To capture the shock wave, the present method employs the quasiconservative form of Jameson's rotated differencing scheme.[16-18] The idea of the quasiconservative scheme is to add the numerical viscosity terms in divergence form to the potential equation written in quasilinear form (nonconservation form). The validity of using the quasiconservative scheme for calculating the unsteady transonic flowfield including the moving shock wave has been examined in Refs. 13 and 15. In these references, it has been shown that the shock motion on the thickening and thinning circular-arc airfoil (maximum thickness is 10% and $M_\infty = 0.85$), which is the severe test of the shock-capturing capability of the schemes, can be well predicted by the quasiconservative scheme.‡

In order to facilitate the rotated differencing scheme, the basic equation (1) is rewritten in canonical form by introducing the local flow coordinate s, which is taken in the direction of the local velocity vector. Then, Eq. (1) becomes

$$(a^2-q^2)\phi_{ss}+a^2(\nabla^2\phi-\phi_{ss})-2q\phi_{st}-\phi_{tt}=0 \tag{10}$$

where ϕ_{ss}, $\nabla^2\phi$, and ϕ_{st} are defined by

$$\phi_{ss}=(1/q^2)(U^2\phi_{xx}+V^2\phi_{yy}+W^2\phi_{zz}+2UV\phi_{xy}+2VW\phi_{yz}+2UW\phi_{xz}) \tag{11}$$

$$\nabla^2\phi=\phi_{xx}+\phi_{yy}+\phi_{zz} \tag{12}$$

$$\phi_{st}=(U/q)\phi_{xt}+(V/q)\phi_{yt}+(W/q)\phi_{zt} \tag{13}$$

respectively. The terms ϕ_{ss}, $\nabla^2\phi$, and ϕ_{st} given in the above can be expressed easily in terms of the variables ξ, η, and ζ in the computational space.

The idea of the quasiconservative scheme is to add the numerical viscosity terms in divergence form to $(a^2-q^2)\phi_{ss}$ term in Eq. (10). Then, Eq. (10) is rewritten as

$$(a^2-q^2)\phi_{ss}+\Delta\xi\frac{\partial F}{\partial\xi}+\Delta\eta\frac{\partial G}{\partial\eta}+\Delta\zeta\frac{\partial H}{\partial\zeta}+a^2(\nabla^2\phi-\phi_{ss})-2q\phi_{st}-\phi_{tt}=0 \tag{14}$$

where F, G, and H are defined by

$$F=\mu(U^2\phi_{xx}+UV\phi_{xy}+UW\phi_{xz})$$

$$G=\mu(V^2\phi_{yy}+UV\phi_{xy}+VW\phi_{yz})$$

$$H=\mu(W^2\phi_{zz}+WU\phi_{xz}+WV\phi_{yz}) \tag{15}$$

where the switching function μ is defined by

$$\mu=\max[0;\ 1-(a/q)^2] \tag{16}$$

The finite difference equations for Eq. (14) of the two-step semi-implicit time-marching technique can be written as follows. The difference equation of the first semi-implicit predictor step for the unknown intermediate potential $\tilde{\phi}_{i,j,k}$ is

$$\begin{aligned}&[(a/q)^2-1][U^2(\phi_{xx})^n_{i,j,k}+V^2(\phi_{yy})^n_{i,j,k}+W^2(\phi_{zz})^n_{i,j,k}\\&+2UV(\phi_{xy})^n_{i,j,k}+2VW(\phi_{yz})^n_{i,j,k}+2UW(\phi_{xz})^n_{i,j,k}]\\&+F^n_{i,j,k}-F^n_{i-1,j,k}+G^n_{i,j,k}-G^n_{i,j\mp1,k}+H^n_{i,j,k}-H^n_{i,j,k\mp1}\\&+(a/q)^2[(q^2-U^2)(\phi_{xx})^n_{i,j,k}+(q^2-V^2)(\tfrac{1}{2})((\tilde{\phi}_{yy})_{i,j,k}\\&+(\phi_{yy})^{n-1}_{i,j,k})+(q^2-W^2)(\phi_{zz})^n_{i,j,k}-2UV(\phi_{xy})^n_{i,j,k}\\&-2VW(\phi_{yz})^n_{i,j,k}-2UW(\phi_{xz})^n_{i,j,k}]-2U(\tilde{\phi}_{xt})_{i,j,k}\\&-2V(\tilde{\phi}_{yt})_{i,j,k}-2W(\phi_{zt})^n_{i,j,k}-(\tilde{\phi}_{tt})_{i,j,k}=0\end{aligned} \tag{17}$$

In the above, $(\phi_{xx})^n_{i,j,k}$, $(\phi_{yy})^n_{i,j,k}$, $(\tilde{\phi}_{yy})_{i,j,k}$, $(\tilde{\phi}_{xt})_{i,j,k}$...,etc. are defined by

$$\begin{aligned}(\phi_{xx})^n_{i,j,k}&=f_{i,k}\overleftarrow{\delta_\xi}(f_{i+\frac{1}{2},k}\overrightarrow{\delta_\xi}\phi^n_{i,j,k})\\(\phi_{yy})^n_{i,j,k}&=g_j\overleftarrow{\delta_\eta}(g_{j+\frac{1}{2}}\overrightarrow{\delta_\eta}\phi^n_{i,j,k})\\(\tilde{\phi}_{yy})_{i,j,k}&=g_j\overleftarrow{\delta_\eta}(g_{j+\frac{1}{2}}\overrightarrow{\delta_\eta}\tilde{\phi}_{i,j,k})\\(\phi_{zz})^n_{i,j,k}&=h_{1i,k}\overleftarrow{\delta_\xi}(h_{1i+\frac{1}{2},k}\overrightarrow{\delta_\xi}\phi^n_{i,j,k})+h_{1i,k}h_{3k}\delta_\xi\delta_\zeta\phi^n_{i,j,k}\\&\quad+h_{3k}\delta_\zeta(h_{1i,k}\delta_\xi\phi^n_{i,j,k})+h_{3k}\overleftarrow{\delta_\zeta}(h_{3k+\frac{1}{2}}\overrightarrow{\delta_\zeta}\phi^n_{i,j,k})\end{aligned} \tag{18}$$

$$\begin{aligned}(\phi_{xy})^n_{i,j,k}&=f_{i,k}g_j\delta_\xi\delta_\eta\phi^n_{i,j,k}\\(\phi_{yz})^n_{i,j,k}&=g_jh_{1i,k}\delta_\xi\delta_\eta\phi^n_{i,j,k}+g_jh_{3k}\delta_\eta\delta_\zeta\phi^n_{i,j,k}\\(\phi_{xz})^n_{i,j,k}&=f_{i,k}\overleftarrow{\delta_\xi}(h_{1i+\frac{1}{2},k}\overrightarrow{\delta_\xi}\phi^n_{i,j,k})+f_{i,k}h_{3k}\delta_\xi\delta_\eta\phi^n_{i,j,k}\end{aligned} \tag{19}$$

$$\begin{aligned}(\tilde{\phi}_{xt})_{i,j,k}&=f_{i-\frac{1}{2},k}(\overleftarrow{\delta_\xi}\tilde{\phi}_{i,j,k}-\overleftarrow{\delta_\xi}\phi^n_{i,j,k})/\Delta t\\(\tilde{\phi}_{yt})_{i,j,k}&=g_{j-\frac{1}{2}}(\overleftarrow{\delta_\eta}\tilde{\phi}_{i,j,k}-\overleftarrow{\delta_\eta}\phi^n_{i,j,k})/\Delta t\quad V\geq0\\&=g_{j+\frac{1}{2}}(\overrightarrow{\delta_\eta}\tilde{\phi}_{i,j,k}-\overrightarrow{\delta_\eta}\phi^n_{i,j,k})/\Delta t\quad V<0\\(\phi_{zt})^n_{i,j,k}&=\overleftarrow{\delta_t}(h_{1i-\frac{1}{2},k}\overleftarrow{\delta_\xi}\phi^n_{i,j,k}+h_{3k-\frac{1}{2}}\overleftarrow{\delta_\zeta}\phi^n_{i,j,k})\quad W\geq0\\&=\overleftarrow{\delta_t}(h_{1i-\frac{1}{2},k}\overleftarrow{\delta_\xi}\phi^n_{i,j,k}+h_{3k+\frac{1}{2}}\overrightarrow{\delta_\zeta}\phi^n_{i,j,k})\quad W<0\\(\tilde{\phi}_{tt})_{i,j,k}&=(\tilde{\phi}_{i,j,k}-2\phi^n_{i,j,k}+\phi^{n-1}_{i,j,k})/\Delta t^2\end{aligned} \tag{20}$$

And the velocities U, V, and W are given by

$$\begin{aligned}U&=f_{i,k}\delta_\xi\phi^n_{i,j,k}+\cos\alpha\\V&=g_j\delta_\eta\phi^n_{i,j,k}+\sin\alpha\\W&=h_{1i,k}\delta_\xi\phi^n_{i,j,k}+h_{3k}\delta_\zeta\phi^n_{i,j,k}\end{aligned} \tag{21}$$

The total velocity q and local sound velocity a can be evaluated by using these U, V, and W. In the above equations, the difference operators such as $\overleftarrow{\delta_\xi}$, $\overrightarrow{\delta_\xi}$, δ_ξ, $\overleftarrow{\delta_\eta}$, $\overrightarrow{\delta_\eta}$,..., etc., follows the standard finite difference notations. For example, $\overleftarrow{\delta_\xi}$, $\overrightarrow{\delta_\xi}$, and δ_ξ are upwind, downwind, and centered difference operator in the ξ direction, respectively.

In Eq. (17), $F^n_{i,j,k}$, $G^n_{i,j,k}$, and $H^n_{i,j,k}$ are given by

$$\begin{aligned}F^n_{i,j,k}&=\mu_{i,j,k}[U^2(\phi_{xx})^n_{i,j,k}+UV(\phi_{xy})^n_{i,j,k}+UW(\phi_{xz})^n_{i,j,k}]\\G^n_{i,j,k}&=\mu_{i,j,k}[V^2(\phi_{yy})^n_{i,j,k}+UV(\phi_{xy})^n_{i,j,k}+VW(\phi_{yz})^n_{i,j,k}]\\H^n_{i,j,k}&=\mu_{i,j,k}[W^2(\phi_{zz})^n_{i,j,k}+WU(\phi_{xz})^n_{i,j,k}+WV(\phi_{yz})^n_{i,j,k}]\end{aligned} \tag{22}$$

‡Further evidence showing the validity of the present finite difference scheme, is presented in Ref. 10, in which the unsteady pressure distributions on a horizontal tail model (NORA WING) oscillating in pitch are compared with the experimental data.

And $G_{i,j\mp 1,k}$ in Eq. (17) means $G_{i,j-1,k}$ for $V\geq 0$ and $G_{i,j+1,k}$ for $V<0$. Similarly, $H_{i,j,k\mp 1}$ means $H_{i,j,k-1}$ for $W\geq 0$ and $H_{i,j,k+1}$ for $W<0$.

It should be noted that the difference expressions of $(\phi_{yy})^n_{i,j,k}$, $(\phi_{xy})^n_{i,j,k}$,..., etc., given in Eqs. (18-21) must be modified for the grid points near and on the wake region ($\eta=0$, $\xi>1$, $0\leq\zeta\leq 1$) so that the potential jump across the wake, which is determined by the wake boundary condition [Eq. (6)], is properly taken into account.

It can easily be confirmed that Eq. (17) leads to the tridiagonal equation with respect to $\tilde{\phi}_{i,j,k}$ ($j=2,\ldots, JZ-1$) for some fixed values of i and k. Therefore, the unknown potential $\tilde{\phi}_{i,j,k}$ at all the grid points inside the boundary can be found by sweeping the tridiagonal equations from upstream to downstream for each value of k (from root chord station to far spanwise direction).

For the second corrector step, the following difference equation is used:

$$
\begin{aligned}
&[(a/q)^2-1]\,[U^2(\phi_{xx})^{n+1}_{i,j,k}+V^2(\phi_{yy})^n_{i,j,k}+W^2(\phi_{zz})^n_{i,j,k}\\
&\quad+2UV(\phi_{xy})^n_{i,j,k}+2VW(\phi_{yz})^n_{i,j,k}+2UW(\phi_{xz})^n_{i,j,k}]\\
&\quad+F^{n+1}_{i,j,k}-F^{n+1}_{i,j,k}+G^n_{i,j,k}-G^n_{i,j\mp 1,k}+H^n_{i,j,k}-H^n_{i,j,k\mp 1}\\
&\quad+(a/q)^2[(q^2-U^2)(\phi_{xx})^n_{i,j,k}+(q^2-V^2)(\phi_{yy})^{n+1}_{i,j,k}\\
&\quad+(q^2-W^2)(\phi_{zz})^{n+1}_{i,j,k}-2UV(\phi_{xy})^n_{i,j,k}-2VW(\phi_{yz})^n_{i,j,k}\\
&\quad-2UW(\phi_{xz})^n_{i,j,k}]-2U(\phi_{xt})^{n+1}_{i,j,k}-2V(\phi_{yt})^{n+1}_{i,j,k}\\
&\quad-2W(\phi_{zt})^{n+1}_{i,j,k}-(\phi_{tt})^{n+1}_{i,j,k}=0
\end{aligned}
\tag{23}
$$

where $F^{n+1}_{i,j,k}$ is defined by

$$
F^{n+1}_{i,j,k}=\mu_{i,j,k}[U^2(\phi_{xx})^{n+1}_{i,j,k}+UV(\phi_{xy})^n_{i,j,k}+UW(\phi_{xz})^n_{i,j,k}] \tag{24}
$$

and where the difference expressions for $(\phi_{zz})^{n+1}_{i,j,k}$ and $(\phi_{zt})^{n+1}_{i,j,k}$, which are somewhat different from the definitions given by Eqs. (18) and (20), respectively, are defined by

$$
\begin{aligned}
(\phi_{zz})^{n+1}_{i,j,k}&=h_{1i,k}\overleftarrow{\delta}_\xi(h_{1i+\frac{1}{2},k}\overrightarrow{\delta}_\xi\phi^n_{i,j,k})+h_{1i,k}h_{3k}\delta_\xi\delta_\zeta\phi^n_{i,j,k}\\
&\quad+h_{3k}\delta_\zeta(h_{1i,k}\delta_\xi\phi^n_{i,j,k})+h_{3k}\overleftarrow{\delta}_\zeta(h_{3k+\frac{1}{2}}\overrightarrow{\delta}_\zeta\phi^{n+1}_{i,j,k})\\
(\phi_{zt})^{n+1}_{i,j,k}&=\overleftarrow{\delta}_t(h_{1i-\frac{1}{2},k}\overleftarrow{\delta}_\xi\phi^n_{i,j,k}+h_{3k-\frac{1}{2}}\overleftarrow{\delta}_\zeta\phi^{n+1}_{i,j,k})\quad W\geq 0\\
&=\overleftarrow{\delta}_t(h_{1i-\frac{1}{2},k}\overleftarrow{\delta}_\xi\phi^n_{i,j,k}+h_{3k+\frac{1}{2}}\overrightarrow{\delta}_\zeta\phi^{n+1}_{i,j,k})\quad W<0
\end{aligned}
\tag{25}
$$

This second step is effectively implicit in the sense that all the leading terms in Eq. (23), namely $(U/q)^2\phi_{xx}$ in ϕ_{ss} [see Eq. (11)] and F [see Eq. (15)], $(1/q^2)(U^2+W^2)\phi_{yy}$ and $(1/q^2)(U^2+V^2)\phi_{zz}$ in the $(\nabla^2\phi-\phi_{ss})$ term [see Eqs. (11) and (12)], $2q\phi_{st}$, and ϕ_{tt} are differenced implicitly (differenced at time level $n+1$). It should be noted here that $\tilde{\phi}$ determined from the first predictor step is incorporated into the difference expressions $[(\phi_{xx})^{n+1}_{i,j,k}, (\phi_{yy})^{n+1}_{i,j,k},\ldots,$ etc.] at the time level $n+1$ in Eq. (23) in the following manner. For example, $(\phi_{xx})^{n+1}_{i,j,k}$ and $(\phi_{yy})^{n+1}_{i,j,k}$ are defined by

$$
\begin{aligned}
(\phi_{xx})^{n+1}_{i,j,k}&=f_{i,k}[f_{i+\frac{1}{2},k}(\tilde{\phi}_{i+1,j,k}-\phi^{n+1}_{i,j,k})\\
&\quad-f_{i-\frac{1}{2},k}(\phi^{n+1}_{i,j,k}-\phi^{n+1}_{i-1,j,k})]/\Delta\xi^2
\end{aligned}
\tag{26}
$$

and

$$
\begin{aligned}
(\phi_{yy})^{n+1}_{i,j,k}&=g_j[g_{j+\frac{1}{2}}(\tilde{\phi}_{i,j+1,k}-\phi^{n+1}_{i,j,k})\\
&\quad-g_{j-\frac{1}{2}}(\phi^{n+1}_{i,j,k}-\phi^{n+1}_{i,j-1,k})]/\Delta\eta^2
\end{aligned}
\tag{27}
$$

respectively. This means that, among the advance values of ϕ (at time level $n+1$) at the neighboring points of (i,j,k), those at the points $(i+1,j,k)$, $(i,j+1,k)$, $(i,j,k+1)$,..., etc., which are not yet passed by the second corrector step, are those calculated by the first predictor step. In this manner, the similar difference expressions for $(\phi_{zz})^{n+1}_{i,j,k}$, $(\phi_{yt})^{n+1}_{i,j,k}$, and $(\phi_{zt})^{n+1}_{i,j,k}$ in which $\tilde{\phi}$ is incorporated can be obtained easily by using the definitions of Eqs. (18-20) and (25). Thus, the unknown potential $\phi^{n+1}_{i,j,k}$ is found simply by a point inversion using the known advance values of the neighboring points, which are available partly from the first predictor step and partly from the second corrector step itself. This point inversion is swept from upstream to downstream in the ξ direction, from bottom to top in the η direction, and from inboard to outboard in the ζ direction.

Although this two-step scheme is still conditionally stable, the addition of the second implicit (not exactly implicit but effectively implicit) step increases the allowable time step size considerably over the scheme that uses only the first semi-implicit sweep. It also should be noted that the present scheme is formally first-order accurate in time.

Boundary Conditions

The flow tangency condition [Eq. (5)] is satisfied on the time mean contour of the wing surface with a technique similar to one used by Carlson[19] in his two-dimensional full potential approach utilizing the Cartesian grid system (see Ref. 10 for details).

The wake boundary condition of Eq. (6) can be rewritten in terms of ξ, η, and ζ as

$$
\Delta\phi_t+f\Delta\phi_\xi=0 \quad \text{on} \quad \eta=0,\ \xi\geq 1,\ 0\leq\zeta\leq 1 \tag{28}
$$

Using this equation, the potential jump across the wake can be given by the following finite difference form:

$$
\begin{aligned}
\Delta\phi^{n+1}_{i,k}&=[\Delta\phi^n_{i,k}+f_{i-\frac{1}{2},k}(\Delta t/\Delta\xi)\Delta\phi^{n+1}_{i-1,k}]\\
&\quad\div[1+f_{i-\frac{1}{2},k}(\Delta t/\Delta\xi)]
\end{aligned}
\tag{29}
$$

Once the value of $\Delta\phi^{n+1}_{i,k}$ at the trailing edge of some spanwise station ($\zeta=k\Delta\zeta$) is determined, the $\Delta\phi^{n+1}_{i,k}$ at all the streamwise grid points in the wake region can be calculated from Eq. (29).

The symmetry conditon of $W=0$ [Eq. (7)] to be satisfied at $z=0$ plane can be rewritten in terms of ξ, η, and ζ as

$$
h_1\phi_\xi+h_3\phi_\zeta=0, \qquad \zeta=0 \tag{30}
$$

In order to satisfy Eq. (30), dummy points are introduced just outside of the symmetry plane.[10] Then ϕ_ξ in Eq. (30) is evaluated by the following second-order difference form at time level n:

$$
\phi_\xi=(\phi^n_{i+1,j,k}-\phi^n_{i-1,j,k})/(2\Delta\xi) \tag{31}
$$

And then ϕ_ζ is expressed by the first-order difference form at time level n as

$$
\phi_\zeta=(\phi^n_{i,j,k}-\phi^n_{i,j,k-1})/\Delta\zeta \tag{32}
$$

Substituting Eqs. (31) and (32) into Eq. (29), the following expressions for the potentials at the dummy points are obtained:

$$
\phi^n_{i,j,k-1}=\phi^n_{i,j,k}+\tfrac{1}{2}(h_{1i,k}/h_{3k})(\Delta\zeta/\Delta\xi)(\phi^n_{i+1,j,k}-\phi^n_{i-1,k}) \tag{33}
$$

The pressures acting on the wing are evaluated on the time mean contour of the wing surface by using Eq. (4), in which ϕ_t and q are evaluated by interpolation from the neighboring grid points.

Numerical Examples

The validation of the present code for 3D wings without control surfaces is explained in Ref. 10. For steady supercritical flows, the pressure distributions calculated by the present code on the ONERA M-6 wing are compared with those predicted by Jameson's fully conservative full potential code[20] and with the experimental data.[21] For unsteady supercritical flows, the unsteady pressure distributions on a horizontal tail model (NORA wing[22]) oscillating in pitch are compared with the experimental data. For both cases, the results obtained by present method showed satisfactory agreement with those of the existing theories and experimental data. In the present paper, therefore, we will present the numerical examples that validate the present code for 3D wings with oscillating control surfaces.

The first example is the NLR swept tapered wing[2] with an oscillating inboard control surface. For this wing, the experimental data measured at subcritical Mach numbers[2] and the theoretical results obtained by the subsonic lifting surface theories of Zwaan[2] and Marchbank[3] are available. The aspect ratio of this wing is 1.53. The leading-edge sweep angle is 50.1 deg and the taper ratio 0.573. The quater-chord length control surface is extended from the root chord station to the 59% semispan station. Since the main purpose of the present numerical calculation for this wing is to compare our results with those of the subsonic lifting surface theories, it is assumed that the airfoil thickness is zero and the amplitude of the control surface oscillation is 0.1 deg. The total number of grid points employed is $47\times51\times17$, among which 25×11 are on the wing and 6×6 are on the control surface. The far-field boundaries are located at 5 chords upstream from the leading edge and 10 chords downstream from the trailing edge in the streamwise direction, 20 chords up and down from the wing surface in the vertical direction, and 4 semispans away from the tip in the spanwise direction. (Exactly the same locations of the far-field boundaries were also used in the subsequent examples). The time step size Δt is about 0.0469. The computation time is about 2.55 s per time step on a FACOM M-380 computer with this number of grid points.

The unsteady calculation is performed at $M_\infty=0.80$, $\alpha=0$ deg, and $k=0.5586$ (which corresponds with $\nu=0.672$, the reduced frequency based on the semispan). For this value of the reduced frequency, about 240 time steps are necessary per cycle of oscillation and 5 cycles of oscillation have been enough to obtain the periodic solution. In Fig. 3, the chordwise distributions of the in-phase and out-of-phase components of the first harmonics of the unsteady aerodynamic loadings at two spanwise stations are plotted and compared with those predicted by the subsonic lifting surface theories of Zwaan[2] (NLR theory) and of Marchbank[3] (BAC theory) and with the experimental data obtained at NLR.[2] The agreement of the present finite difference calculations with those of the two subsonic lifting surface theories and with the experimental data is satisfactory at all of the spanwise stations considered.

The second example is for testing the capability of the present code for calculating supercritical flows. The wing we have calculated is the RAE swept tapered wing with a part-span control surface, for which the experimental data obtained by Mabey et al.,[23] are available. The planform of the RAE wing is shown in Fig. 4. The aspect ratio of the wing is 6, taper ratio ⅓, and the leading-edge sweep angle 36.7 deg. The hinge line of the control surface is located through the 70% chord position and the side edges of the control surface are located at 40% and 70% semispan stations, respectively. The streamwise airfoil section of this wing is the 9% RAE 101 section. The total number of grid points is $47\times51\times19$, among which 25×13 are on the wing and 7×5 are on the control surface. The computation time is about 2.85 s per time step on a FACOM M-380 computer with this number of grid points. The time step size Δt used for this problem was about 0.04. The finite difference calculations have been performed

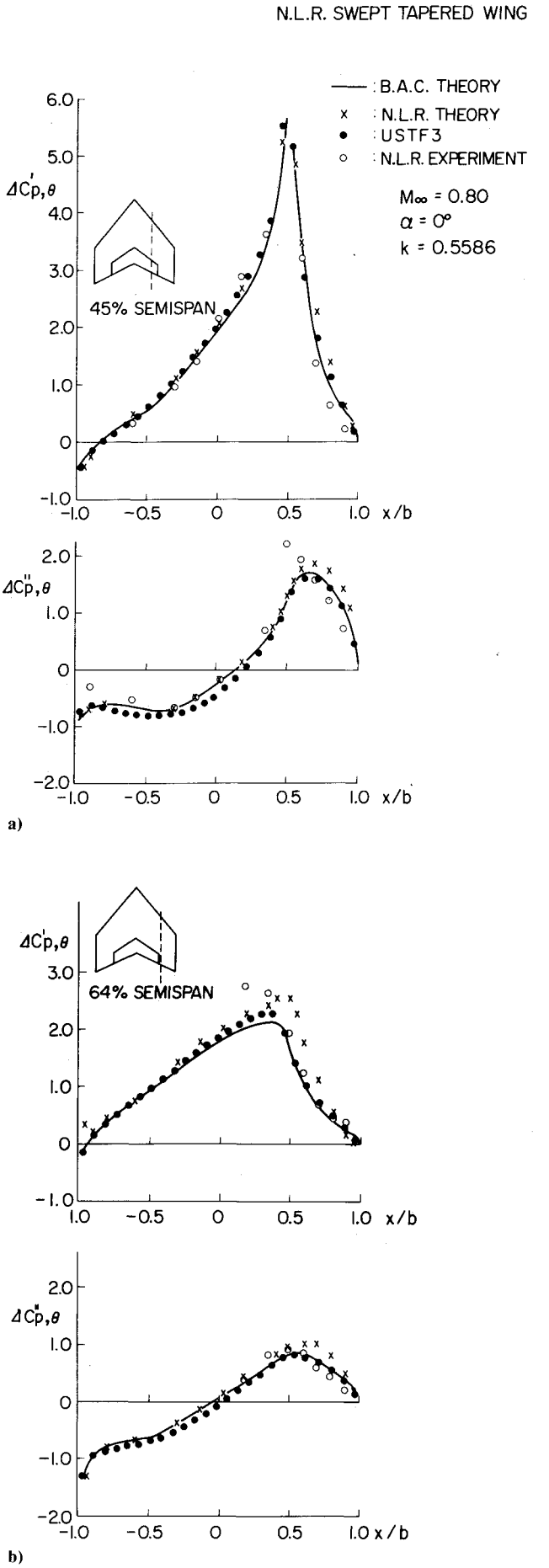

Fig. 3 Unsteady load distributions (first harmonics) on NLR swept tapered wing with oscillating inboard control surface.

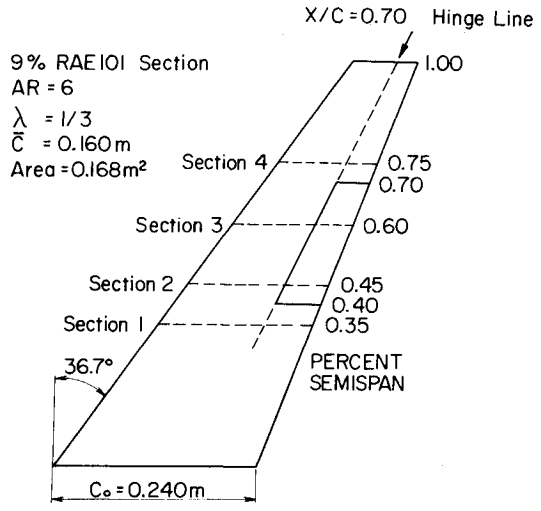

Fig. 4 Planform of RAE swept tapered wing.[23]

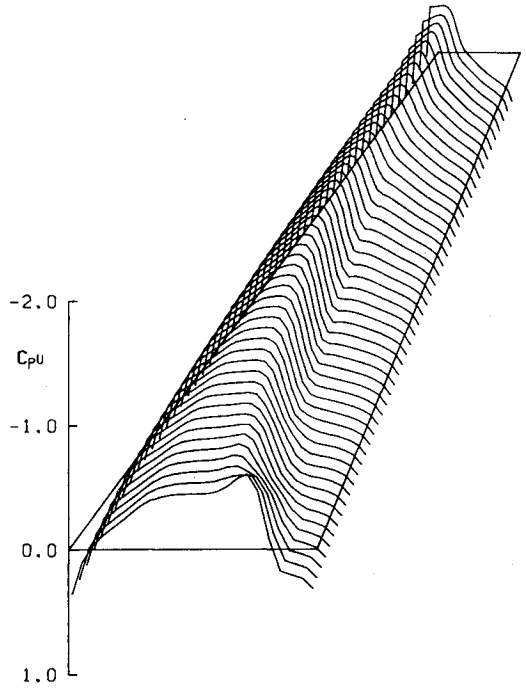

Fig. 5a Chordwise and spanwise steady-state pressure distributions on RAE swept tapered wing at $M_\infty = 0.90$ and $\alpha = 0$ deg.

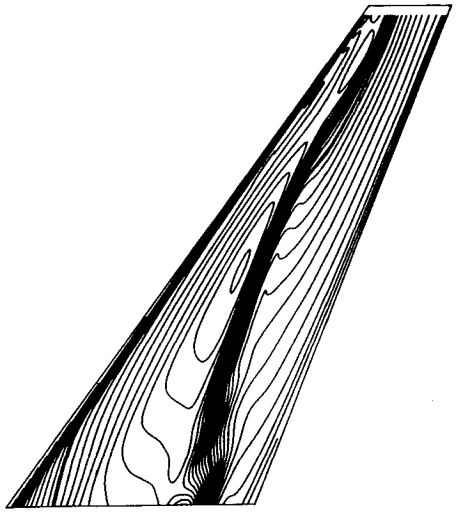

Fig. 5b Isobar pattern of the steady-state pressure on RAE swept tapered wing at $M_\infty = 0.90$ and $\alpha = 0$ deg.

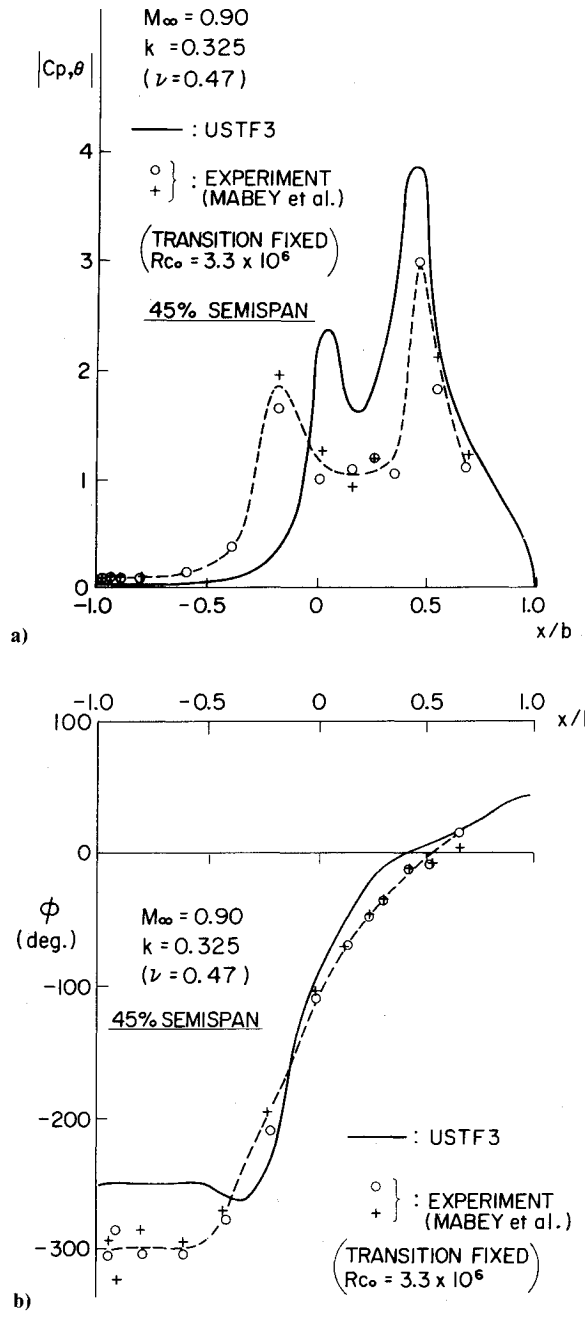

Fig. 6 Calculated and experimental unsteady pressure distributions (first harmonics) on upper surface of RAE swept tapered wing with oscillating part-span control surface: a) magnitude, b) phase angle.

for $M_\infty = 0.90$ and $\alpha = 0$ deg. The reduced frequency of the control surface oscillation is $k = 0.3250$ ($\nu = 0.47$, the reduced frequency based on the mean aerodynamic chord[23]) and about 483 time steps are necessary per cycle of oscillation. The amplitude of the control surface oscillation was 1 deg for both the experiment and the calculation.

The chordwise and spanwise steady-state pressure distributions and the corresponding isobar pattern are shown in Fig. 5. In these figures it is seen that the shock wave extends from about a 80% chord position at the root chord station to a 35% chord position at the tip station. These calculated steady-state pressure distributions are not compared with the experimental data, which are not available in Ref. 23. A total of seven cycles of oscillation have been necessary to obtain the periodic solution of the oscillating control surface problem. The chordwise distributions of the magnitude and phase angles of the first harmonics of the unsteady pressure distributions on the upper surface at the 45% semispan

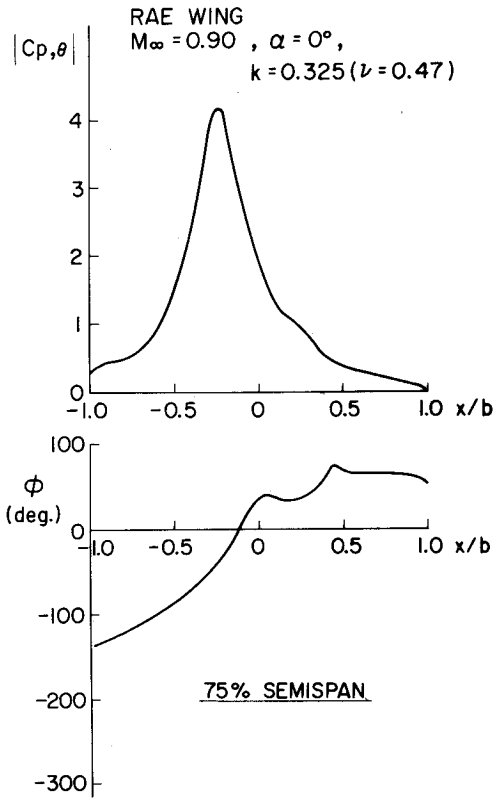

Fig. 7 Calculated unsteady pressure distributions (first harmonics) on upper surface of RAE swept tapered wing with oscillating part-span control surface.

station are plotted and compared with the experimental data obtained by Mabey et al.[23] in Fig. 6. In both the theoretical and experimental data, two peaks are observed in the magnitude distributions. The first peak values, which are observed at about the 40% chord position in the experimental data and the 50% chord position in the calculated results, respectively, are due to the oscillation of the shock wave; and the second peak values observed around the 70% chord position in both the experimental and theoretical results are due to the singularities existing at the hinge line. The discrepancy in the magnitude of the first peak values between the theory and experiment clearly comes from the difference of the shock wave locations between the two. That is, the shock location in the experiment is about the 10% chord upstream compared with that of the theory. This disparity between the computed and experimental results can well be explained by the viscous ramp concept. The displacement thickness of the turbulent boundary layer changes slope abruptly, owing to the large adverse pressure gradient near the base of the shock wave. Therefore, the viscous flow near a shock wave corresponds locally to the inviscid flow over a sharp-nosed edge. This wedge converts the normal shock of a purely inviscid solution into a weaker shock and displaces it upstream from the purely inviscid location. This sort of viscous effect is more pronounced at low Reynolds numbers such as those of the cited experiment ($R_{C_0} = 3.3 \times 10^6$).

In Fig. 7, the chordwise distributions of the magnitude and phase angle of the first harmonic components of the calculated unsteady pressure distributions at the 75% semispan station are plotted, although the experimental data at this semispan station are not reported in Ref. 23. It is interesting to see that the relatively large peak value in the magnitude of the unsteady pressure variation is induced by the oscillation of the shock wave at this semispan station, which is off the control surface location (see Fig. 4). This phenomenon can be seen more clearly in Fig. 8 where the chordwise and spanwise distributions of the in-phase and out-

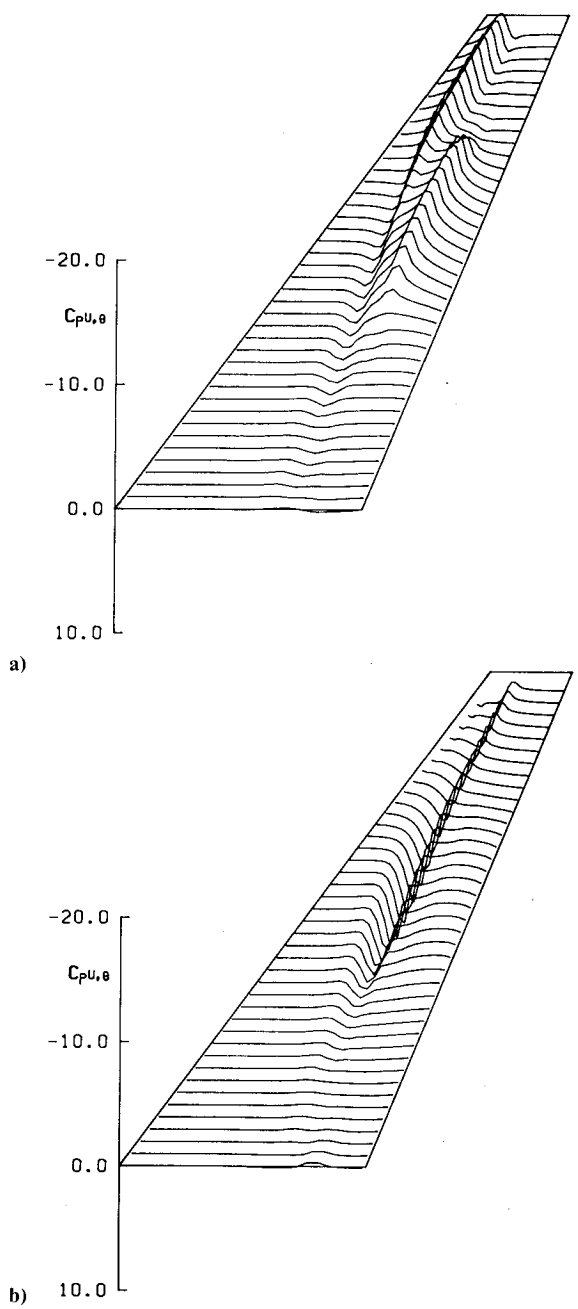

Fig. 8 Chordwise and spanwise unsteady pressure distributions (first harmonics) on RAE swept tapered wing with oscillating part-span control surface ($M_\infty = 0.90$, $\alpha = 0$ deg, $k = 0.325$, ($\nu = 0.47$)): a) real part, b) imaginary part.

of-phase components of the unsteady upper surface pressure are plotted. The first peak values (observed in Fig. 8), ranging from the midsemispan stations to the tip station with increasing strength, are due to the shock wave oscillation and the second peak values ranging from about the 40% semispan to the 70% semispan station are due to the singularities existing on the hinge line of the control surface.

Conclusions

Numerical calculations of unsteady transonic flow over three-dimensional wings with oscillating control surfaces have been performed. For this purpose, the computer code USTF3, which solves the unsteady three-dimensional full potential equation by a two-step semi-implicit time-marching finite difference technique and which was originally developed by the present authors, has been modified by introducing the new grid system that is appropriate for solving control surface

problems. In order ot evaluate the code the unsteady pressure distributions on the NLR swept tapered wing with an inboard control surface and on the RAE swept tapered wing with a part-span control surface have been calculated and compared with those of the existing theories and experimental data.

Agreement of the unsteady pressure distributions on the NLR wing between the present calculations and the subsonic lifting surface theories was satisfactory for the subcritical Mach number. For the pressure distributions on the RAE swept tapered wing, there have been observed some quantitative discrepancies for the supercritical Mach number between the present calculations and the experimental data, which may be attributed to the effects of the shock wave and turbulent boundary-layer interactions, although the qualitative behavior of the unsteady pressure distributions has been well predicted by the present method. A modification of the present code USTF3 to take into account the effects of the turbulent boundary-layer interactions is now under investigation.

An immediate application of the present code, which also has a capability of calculating the time-dependent aeroelastic response of a flexible wing as demonstrated in Ref 12, is a time-domain numerical simulation of active control systems such as flutter suppression systems. Such an example is given in Ref. 14.

References

[1] Ashley, H. and Rowe, W. S., "Unsteady Aerodynamic Loading of Wings with Control Systems," *Zeitschrift fuer Flugwissenshaften*, Vol. 18, Sept.-Oct. 1970, pp. 321-330.

[2] Zwaan, R. J., "On a Kernel-Function Method for the Calculation of Pressure Distribuitons on Wings with Harmonically Oscillating Control Surfaces in Subsonic Flow," NLR TR/70123U, March 1971.

[3] Marchbank, W. R., "Evaluation of Pressure Distributions on Thin Wings with Distorted Control Surfaces Oscillating Harmonically in Linearized, Compressible, Subsonic Flow, Part I: Details of the Mathematical Techniques Used in the Evaluation of the Pressure Distributions, and a Set of Numerical Results including Comparisons with Experiment," RAE R&M No. 3783, 1976.

[4] Rowe, W. S., Winther, B. A., and Redman, M. C., "Unsteady Subsonic Aerodynamic Loadings Caused by Control Surface Motions," *Journal of Aircraft*, Vol. 11, Jan. 1974, pp. 45-54.

[5] Borland, C. J., Rizzetta, D. P., and Yoshihara, H., "Numerical Solution of Three Dimensional Unsteady Transonic Flow Over Swept Wings," *AIAA Journal*, Vol. 20, March 1982, pp. 340-347.

[6] Borland, C. J. and Rizzetta, D. P., "Nonlinear Transonic Flutter Analysis," *AIAA Journal*, Vol. 20, Nov. 1982, pp. 1606-1615.

[7] Rizzetta, D. P. and Borland, C. J., "Numerical Solution of Three-Dimensional Unsteady Transonic Flow over Wings Including Inviscid/Viscous Interaction," AIAA Paper 82-0352, Jan. 1982.

[8] Couston, M. P. and Angelini, J. J., "Extension of the Transonic Perturbation Approach to Three-Dimensional Problems," ONERA, T. P. NO. 1981-147, 1981.

[9] Steger, J. L. and Caradonna, F. X., "A Conservative Implicit Finite Difference Algorithm for the Unsteady Transonic Full Potential Equation," AIAA Paper 80-1368, July 1980.

[10] Isogai, K., "Calculation of Unsteady Transonic Potential Flow over Oscillating Three-Dimensional Wings," National Aerospace Laboratory, Japan, Rept. TR-706T, March 1982.

[11] Sankar, N. L., Malone, J. B., and Tassa, Y., "An Implicit Conservative Algorithm for Steady and Unsteady Three-Dimensional Transonic Potential Flows," AIAA Paper 81-1016, April 1981.

[12] Isogai, K. and Suetsugu, K., "Numerical Simulation of Transonic Flutter of a Supercritical Wing," National Aerospace Laboratory, Japan, Rept. TR-726T, Aug. 1982.

[13] Isogai, K., "Calculation of Unsteady Transonic Flow over Oscillating Airfoils Using the Full Potential Equation," AIAA Paper 77-448, March 1977.

[14] Isogai, K. and Suetsugu, K., "Calculation of Unsteady Transonic Potential Flow over Three-Dimensional Wings with Oscillating Control Surfaces," National Aerospace Laboratory, Japan, Rept. TR-746, Dec. 1982 (in Japanese).

[15] Isogai, K., "Numerical Study of Transonic Flutter of a Two-Dimensional Airfoil," National Aerospace Laboratory, Japan, Rept. TR-617T, June 1980.

[16] Jameson, A., "Transonic Potential Flow Calculations Using Conservation Form," *Second AIAA Conference on Computational Fluid Dynamics*, Hartford, Conn. June. 1975, pp. 148-161.

[17] Bauer, F. and Korn, D., "Computer Simulation of Transonic Flow Past Airfoils with Boundary Layer Correction," *Second AIAA Conference on Computational Fluid Dynamics*, Hartford, Conn., June 1975, pp. 184-204.

[18] Caughey, D. A. and Jameson, A., "Numerical Calculation of Transonic Potential Flow About Wing-Body Combinations," AIAA Paper 77-677, June 1977.

[19] Carlson, L. F., "Transonic Airfoil Flow Field Analysis Using Cartesian Coordinates," NASA CR-2577, Aug. 1975.

[20] Jameson, A. and Caughey, D. A., "A Finite Volume Method for Transonic Potential Flow Calculations," AIAA Paper 77-635, June 1977.

[21] Schmitt, V. and Charpin, F., "Pressure Distributions on the ONERA-M6-WING at Transonic Mach Numbers, Experimental Data Base for Computer Program Assessment," AGARD-AR-138, May 1979, pp. B1-1—B1-44.

[22] Lambourne, N., Destuynder, R., Kienappel, K., and Roos, R., "Comparative Measurements in Four European Wind Tunnels of the Unsteady Pressures on an Oscillating Model (The NORA Experiments)," AGARD Rept. 673, Paper presented at 49th Structures and Materials Panel Meeting, Porz-Wahn, West Germany, Oct. 1979.

[23] Mabey, D. G., McOwat, D. M., and Welsh, B. L., "Aerodynamic Characteristics of Moving Trailing-Edge Controls at Subsonic and Transonic Speeds," *Aerodynamic Characteristics of Controls*, AGARD-CP-262, May 1982, pp. 20-1—20-25.